Earth and Planetary Science Letters 581 (2022) 117393

Contents lists available at ScienceDirect

Earth and Planetary Science Letters

www.elsevier.com/locate/epsl

Potassium incorporation and isotope fractionation in cultured scleractinian corals

Wenshuai Li [a], Xiao-Ming Liu [a,*], Kun Wang [b], Yongfeng Hu [c], Atsushi Suzuki [d], Toshihiro Yoshimura [e]

[a] Department of Earth, Marine and Environmental Sciences, University of North Carolina, Chapel Hill, Chapel Hill, NC 27599-3315, USA
[b] Department of Earth and Planetary Sciences and McDonnell Center for the Space Sciences, Washington University in St. Louis, MO 63130, USA
[c] Canadian Light Source, University of Saskatchewan, Saskatoon, SK S7N 0X4, Canada
[d] Geological Survey of Japan, National Institute of Advanced Industrial Science and Technology, Tsukuba 305-8567, Japan
[e] Japan Agency for Marine-Earth Science and Technology, 2-15, Natsushima-cho, Yokosuka-city, Kanagawa 237-0061, Japan

ARTICLE INFO

Article history:
Received 3 August 2020
Received in revised form 12 January 2022
Accepted 17 January 2022
Available online 4 February 2022
Editor: A. Jacobson

Keywords:
temperature
biomineralization
seawater
XANES
paleoceanography

ABSTRACT

Potassium (K) participates in coral biological activities and accumulates in their skeletons, driving the fractionation of stable K isotopes ($^{41}K/^{39}K$). Constraining the influences of biotic and abiotic controls on K isotope fractionation is important for interpreting coral records. However, the processes and mechanisms regulating K incorporation into coral skeletons and K isotope fractionation between seawater and coral skeletons remain unknown. Here, we combined isotopic and synchrotron-based spectroscopic analyses to evaluate the phase distribution and corresponding isotope variation of K in the skeleton of scleractinian (*Porites australiensis*) corals at a seawater temperature range from 20 to 29 °C in aquaria culture experiments. Potassium in coral skeletons exists mainly as organic-K (K hosted in soluble and insoluble organic matrices) and carbonate-K (K incorporated into K_2CO_3 and aragonite) phases of various proportions. Coral $\delta^{41}K$ values vary substantially in both direction and magnitude from the modern seawater $\delta^{41}K$ composition (~0.12‰), showing marked deviations ($\Delta^{41}K_{Coral\text{-}Sea}$) from −2.00 to 0.67‰. As seawater temperature increases, the organic-K fraction increases, whereas $\delta^{41}K_{Coral}$ decreases. The variation in $\delta^{41}K_{Coral}$ reflects the relative proportions of organic-bound K to carbonate-associated K. In most cases, coral intracrystalline organic matrices preferentially sequester isotopically lighter K whereas carbonate phases prefer heavier K. Distinguishable inter-colony difference in skeletal $\delta^{41}K$ of corals growing under the same culturing conditions reveals the influence of physiological controls on K partitioning and isotope fractionation. Although calcification rate correlates with temperature to different degrees in the studied corals, likely reflecting control of the difference in zooxanthellae density, we infer that calcification rate is not a major controlling factor on skeletal $\delta^{41}K$. Rather, skeletal $\delta^{41}K$ correlates closely with K phase partitioning, which is ascribed to temperature-sensitive physiological modulation.

1. Introduction

Marine biogenic carbonates have been utilized for paleoclimatic and paleoceanographic reconstruction (e.g., coral reefs), and usually produce iconic geological records in the field (Krief et al., 2010; Lesser et al., 2018). The geochemical compositions of well-preserved coral skeletons may provide high-resolution geochemical archives of temporal seawater conditions, and the duration of the record produced ranges from weeks to millions of years (Stan et al., 2017; Gothmann et al., 2017; Montefalcone et al., 2018; Lesser et al., 2018). The use of scleractinian coral archives is ascribed to their habitats in a diverse range from warm, supersaturated, surface waters to cold, deep waters, and they act as "reef builders" for seawater chemistry recording since the start of the Oligocene epoch (Stanley, 1988).

The influence of a wide number of seawater variables including temperature, salinity, ionic speciation, and pH on the elemental and isotopic partitioning between scleractinian corals and seawater has been investigated for decades. Well-established geochemical proxies in scleractinian corals are often used as paleoceanographic toolkits, including skeletal elemental ratios (P/Ca, Sr/Ca, Mg/Ca, and B/Ca) and isotopic compositions ($\delta^{11}B$, $\delta^{18}O$, $\delta^{26}Mg$, and $\delta^{44}Ca$) (Gaetani et al., 2011; Yoshimura et al., 2011; Montagna et al., 2014; Gothmann et al., 2017; McCulloch et al., 2017; M. Chen

* Corresponding author.
E-mail address: xiaomliu@unc.edu (X.-M. Liu).

https://doi.org/10.1016/j.epsl.2022.117393
0012-821X/

et al., 2019). Scleractinian coral proxies have broad implications for reconstructing temperature, pH, and salinity, as well as seawater isotopic values that are used to constrain oceanic isotope mass balances. However, the chemical composition in coral skeletons is affected not only by external environmental conditions but also biological activity, generally referred to as the "vital effect". Efforts to interpret elemental and isotopic signatures archived in coral records need to assess the vital effect, potentially altering how calcified "hard materials" preserve information about seawater chemistry (Sinclair et al., 2006; Stanley, 2008; Elderfield, 2010; Yoshimura et al., 2011; Saenger and Wang, 2014; Gothmann et al., 2017). For example, accelerated calcification may or may not break the elemental and isotopic equilibria (Saenger and Wang, 2014; Inoue et al., 2015; Wall et al., 2019). Physiological modulation on elemental partitioning into various phases in coral skeletons can potentially modify the interpretation of seawater chemistry, as reported for the link between P/Ca and P phase distribution by chemical extraction (M. Chen et al., 2019).

The potassium (K) isotope system has the potential to trace chemical weathering that modulates the long-term atmospheric carbon cycle (Li et al., 2019). The global extent of clay formation and their assemblage strongly modulate the K flux and isotope composition of seawater (Santiago Ramos et al., 2018; Chen et al., 2020; Huang et al., 2020; Li et al., 2019, 2021a; Wang et al., 2021). Due to the long residence time (~10 Myr) of K in the modern ocean compared with that of ocean water (~4,100 yr), ancient seawater K isotope values have the potential for evaluating weathering processes over geological history (Hille et al., 2019; Wang et al., 2020). While biomineralization in marine calcifiers has long been examined (Weiner and Dove, 2003; Stanley, 2008) and marine biogenic carbonates are widely used as high-fidelity proxies of past seawater chemistry (Elderfield, 2010), attempts to understand their K isotope systematics have only recently begun (Li et al., 2021b). Therefore, the reconstruction of seawater K isotopic information from marine carbonates requires evaluation and calibration. However, the reconstruction may be affected by seawater physicochemical property (e.g., temperature or pH), calcification kinetics, the vital effect, and diagenetic alteration (Yoshimura et al., 2011; Saenger and Wang, 2014; Ullmann and Korte, 2015; Gothmann et al., 2017). It is necessary to obtain comprehensive knowledge of how biogenic carbonates preserve seawater δ^{41}K signals.

In this study, we evaluate the potential of *Porites* corals as archives of past seawater δ^{41}K values. The main aims of this study are to (i) determine the distribution and incorporation of K into the skeletons of azooxanthellate scleractinian corals (*Porites australiensis*), including temperature dependence, and (ii) determine the directions, magnitudes, and dominant processes for K isotope fractionation between surrounding seawater and coral skeleton spanning a temperature range from 20 to 29 °C. We conclude that skeletal δ^{41}K value decreases with increasing seawater temperature because the physiological control on K partitioning in the studied corals is highly temperature-sensitive.

2. Materials and methods

Details of the setup of the coral culturing experiments (Figs. S1-S2), sample processing, and analytical methodologies are provided in Supplementary Materials. In brief, two *Porites australiensis* colonies (zooxanthellate scleractinian coral) in aquaria experiments were recovered from a fringing reef offshore close to the southern coast of Sesoko Island, Okinawa, Japan (26°37′N, 127°51′E). We selected colonies growing >10 m apart from each other to ensure their genetic differences. We note that two asexually reproduced colonies (referred to as B and C) were finely separated into multiple 2×2×2 cm^3 cubes at Sesoko Station, the Tropical Biosphere Research Centre at the University of the Ryukyus. Recovered clone colonies (in cubes) were allowed to heal and acclimate in an open-air tank for a 3-week incubation period under moderate sunlight intensity with partial shading using a sunscreen mesh (a reduction by about 24% of ambient sunshine intensity). Before the culture experiment, coral colonies were stained by Alizarin red S and marked (1~18, dependent on the experimental setting). The samples reported in this study belong to a part of the sample set in Hayashi et al. (2013). Colony cubes were transferred into tanks (20.6 L) in semi-open systems inside the laboratory with a continuous supply of aerated Pacific surface seawater and cultured from November 14, 2006 to April 18, 2007. Aeration before the temperature controls should result in the enhanced air/water exchange of CO_2, thus leading to the equilibrium between the air and the culture media. Seawater salinity kept stable throughout the culture period (34.6±0.5, see Fig. 1 in Hayashi et al., 2013). In addition, Suwa et al. (2010), Fujita et al. (2011), and Ohki et al. (2013) have reported the pH and pCO_2 values of tank water after aeration of ambient air (Table S1). The aragonite saturation state of the tank water estimated using the CO2SYS program, ranges from 3.2 to 3.53. These observed values were near equilibrium with ambient air and indicated little or no aeration-induced skeletal growth changes in our culture systems. Hence, we suggest that seawater chemistry likely remained consistent during the culture experiment.

The only biological difference between coral colonies B and C is the higher zooxanthellae density in B, which is important for photoautotrophy (i.e., organisms make their energy via the process of photosynthesis). In the following text, colonies B and C refer to high and low zooxanthellae-density coral types, respectively. The investigated corals contain photoautotrophic dinoflagellates in the tissues called the "zooxanthellae" (Lesser et al., 2018). The symbiosis between the zooxanthellae and the coral hosts is supposed to be mutualistic, and we determined that colony B calcified faster than colony C in culturing systems at the same temperature.

Skeletal powders obtained from 2 to 6 mm were selected for K isotope analysis to prevent potential surface contamination. During sampling, the outermost materials (~2 mm) were carefully removed from samples with a microdrill because it is composed of coral tissues. Samples were ultrasonicated with methanol and rinsed with deionized water three times to remove the remaining surface impurity. Samples were powdered using an agate mortar, treated with deionized water rinses (18.2 MΩ·cm, Millipore™), and ultrasonicated. This step was repeated until the residual solutions were clear and concentrations of dissolved cations (e.g., Fe, Mn, Mg, Al, Li, and K) were below the detection limits of the Q-ICP-MS. The mortar and pestle were washed between samples using 2% HNO_3 and deionized water to avoid cross-contamination. After that, powdered coral samples were treated with NH_4Ac cleaning suggested in Saenger and Wang (2014). This allows for the elimination of exchangeable surface complexes using 1 M NH_4Ac followed by deionized water rinses in triplicate. For oxidative cleaning, coral samples were subjected to two cycles of 5-min ultrasonication and rinsed using a mixed solution of 1:1 v/v 15% H_2O_2 and 0.5% $HClO_4$ (Suzuki et al., 2005; Yoshimura et al., 2011). The reliability of the cleaning steps has been validated in Li et al. (2021b). The presence of organic-ion associations has been reported for nutrient elements (M. Chen et al., 2019; Zhao et al., 2021), causing distinct isotopic composition within bulk carbonates, and the impact of K in organic matter was evaluated. In addition to cultured samples, one *Porites* coral sample (CR-FL-Ps) from Key Largo as a field analog was processed following the same procedure and measured for comparison.

Three types of organic materials generally exist within corals, including outer soft tissues, intercrystalline organic and intracrystalline organic matrices. The first two kinds of organic materials can easily be cleaned. However, lattice-bound (intracrystalline) organic matter cannot be fully removed from the bulk sample (Frei

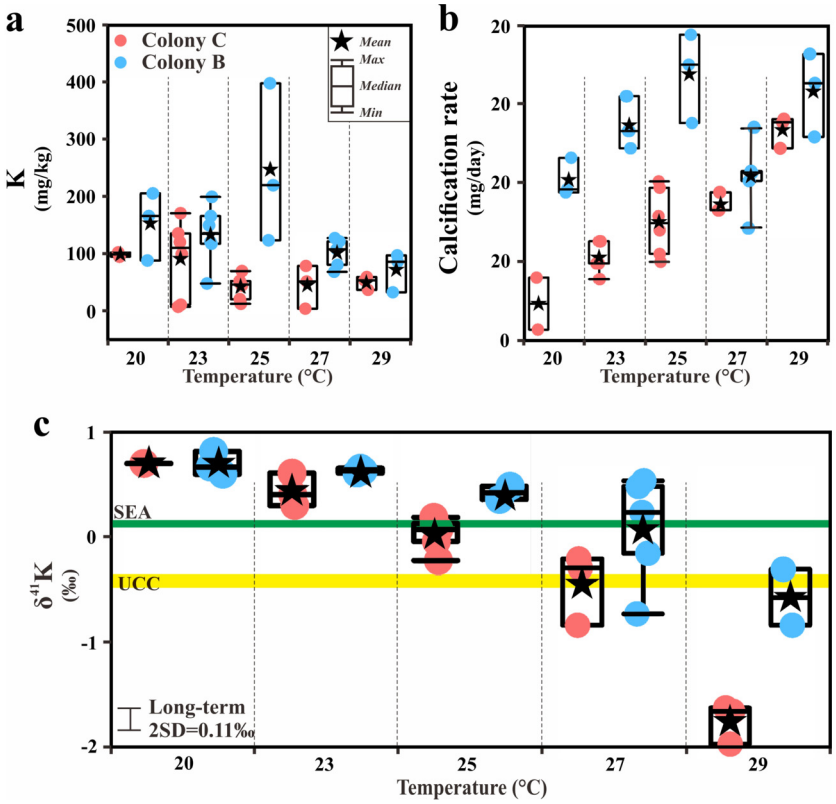

Fig. 1. Geochemical characterization of coral skeletons (colonies B and C), including (a) skeletal K concentration, (b) calcification rate, and (c) isotopic composition (δ^{41}K). The green and yellow bars in the box plot (c) represent the δ^{41}K values of the upper continental crust (UCC, averaged δ^{41}K of -0.44 ± 0.05‰, Huang et al., 2020) and modern seawater (SEA, homogeneous δ^{41}K of ~0.12‰, Hille et al., 2019; Wang et al., 2020), respectively. The long-term uncertainty of isotope analysis using MC-ICP-MS is 0.11‰ (2 S.D.) (Chen et al., 2019). Along the x-axis, coral data are arrayed in a sequence of target temperatures. (For interpretation of the colors in the figure(s), the reader is referred to the web version of this article.)

et al., 2018; Bruggmann et al., 2019). It is necessary to assess the difference in K phases and its isotopic fractionation between Intracrystalline organics and the bulk sample to decipher biological regulation on coral skeletal K isotope composition via organic matter extraction. The procedure of reliable chemical extraction was provided in Yoshimura et al. (2017), and is briefly summarized. A tip of the axial skeleton of corals was immersed into 0.25 M EDTA (pH=7.8) for ~60 h at ~4 °C to demineralize coral $CaCO_3$ frameworks. The soluble organic matrices (OM-K1) extracted from skeletons were collected, and insoluble organic-K matrices (OM-K2) were rinsed with deionized water and dried at 60 °C prior to analysis. After bulk element and K isotope analysis, <10 mg of each cultured coral sample was left. Hence, cultured coral samples were not processed due to their limited sample size, which was insufficient for chemical extraction. Alternatively, we used a field-collected *Porites* coral (CR-FL-Ps) in an extraction experiment to provide complementary information about K associated with intracrystalline organic matter. Although firm interpretations based on field-collected coral may not be made, extracted organic matrices and bulk samples could provide valuable insights into the K phase and its isotopic fractionation in *Porites* coral skeletons.

In the digestion step, 300 mg samples were weighed in 50 mL Teflon® beakers, dissolved using 0.05 M HCl+30% H_2O_2 solutions in a thermostatic oven at 60 °C for over a week, and then transferred to a hotplate set to 120 °C until complete dissolution (Li et al., 2021b). After acid dissolution, released organic matrices (mainly intracrystalline organic matrices) were removed by chemical treatments using 30% H_2O_2 to minimize the interferences on element analysis. After digestion, samples were dissolved in 2% HNO_3 prior to analysis. Elemental concentrations of coral skeletons were measured using an Agilent™ 7900 Q- ICP-MS using a series of internal standards of Be, Ge, Rh, In, Ir, and Bi, at the University of North Carolina at Chapel Hill. Analytical precision for elemental composition (e.g., K, Na, Mg, and Al) is <10% based on repeated measurements of NIST-SRM-1d (limestone) and JCp-1 (*Porites* coral) relative to reported values in the literature (Tables S2 and S3).

Skeletal K speciation was quantified using K *K*-edge X-ray absorption near-edge structure (XANES) spectra processed with linear combination fitting (XANES-LCF) at the Soft X-ray Micro-Characterization beamline (SXRMB) at the Canadian Light Source (Table 1). The XANES analysis was performed on powdered materials that were treated with the same cleaning processes as samples that were dissolved for the K isotope measurement. Because the degree of trace metal incorporation within $CaCO_3$ is controlled primarily by crystal lattice polymorphs, we obtained *K*-edge XANES data of the K atoms in carbonate references (i.e., synthetic K-bearing calcite/aragonite, anhydrous and hydrated forms of K_2CO_3, and commercial $KHCO_3$). The K XANES spectra of seawater and KCl (s) were used to identify dissolved K^+ (e.g., fluid inclusions) and the solid KCl salt phase in coral skeletons if any.

The K isotope compositions of cleaned powdered coral slabs were analyzed using a MC-ICP-MS at the Washington University in St. Louis, expressed in a delta notation (Table 2) (normalization to NIST SRM 3141a) by the following equation:

$$\delta^{41}\mathrm{K}\ (‰) = \left\{ \frac{(^{41}\mathrm{K}/^{39}\mathrm{K})_{\mathrm{sample}}}{(^{41}\mathrm{K}/^{39}\mathrm{K})_{\mathrm{NIST\ SRM\ 3141a}}} - 1 \right\} \times 1000, \quad (1)$$

The reproducibility of K isotope analysis was confirmed using a limestone standard NIST-SRM-1d, a coral standard JCP-2, and two igneous standards BHVO-2 and GSP-2 (Table S4). Repeated mea-

Table 1
Coral skeletal K speciation based on XANES-LCF analysis.

Sample ID	XANES-LCF results					Sum			*R*
	$K_2CO_3 \cdot 1.5H_2O$ (%)	Soluble OM-K1 (%)	K_2CO_3 (%)	Insoluble OM-K2 (%)	Aragonite-K (%)	K hosted in total K_2CO_3 (%)[a]	K hosted in carbonates (%)[b]	K hosted in organic matrices (%)[c]	
Colony C (low zooxanthellae-density)									
C3	7.3 (2.7)	91.5 (5.6)	0.0 (0.0)	1.2 (1.2)	0.0 (0.0)	7.3 (2.7)	7.3 (2.7)	92.7 (5.7)	0.06
C4	8.9 (2.1)	82.2 (6.2)	0.0 (0.0)	2.5 (1.8)	6.4 (3.7)	8.9 (2.1)	15.3 (4.7)	84.7 (6.5)	0.06
C10	13.5 (4.1)	71.2 (7.3)	1.6 (1.6)	7.1 (1.8)	6.6 (3.4)	15.1 (4.4)	21.7 (5.6)	78.3 (7.5)	0.08
C12	20.7 (13.1)	50.6 (10.5)	0.0 (0.0)	28.7 (9.5)	0.0 (0.0)	20.7 (13.1)	20.7 (13.1)	79.3 (14.1)	0.11
C14*	10.5 (6.2)	68.1 (11.4)	5.8 (3.7)	0.0 (0.0)	15.6 (6.3)	16.3 (7.2)	31.9 (9.6)	68.1 (11.4)	0.11
C17	26.4 (6.7)	0.0 (0.0)	5.4 (2.9)	58.0 (4.9)	10.1 (4.3)	31.8 (7.3)	41.9 (8.5)	58.0 (4.9)	0.08
Colony B (high zooxanthellae-density)									
B2	20.7 (13.1)	50.5 (9.4)	0.0 (0.0)	28.8 (9.6)	0.0 (0.0)	20.7 (13.1)	20.7 (13.1)	79.3 (13.4)	0.11
B5	17.4 (6.5)	45.6 (5.2)	5.8 (2.8)	31.2 (4.8)	0.0 (0.0)	23.2 (7.1)	23.2 (7.1)	76.8 (7.1)	0.08
B8	10.4 (4.0)	39.2 (3.3)	9.6 (4.0)	27.1 (3.5)	13.7 (5.4)	20.0 (5.7)	33.7 (7.8)	66.3 (4.8)	0.08
B14	20.2 (6.7)	40.9 (4.4)	0.0 (0.0)	28.0 (4.9)	10.9 (3.1)	20.2 (6.7)	31.1 (7.4)	68.9 (6.6)	0.09
B17	23.3 (4.4)	46.3 (6.7)	8.6 (4.4)	6.4 (2.6)	15.4 (4.1)	31.9 (6.2)	47.3 (7.5)	52.7 (7.2)	0.08
B18	31.7 (4.3)	34.3 (6.6)	8.9 (4.1)	5.4 (2.2)	19.7 (3.8)	40.6 (5.9)	60.3 (7.1)	39.7 (7.0)	0.08

Note 1: [a]a sum of K_2CO_3 and $K_2CO_3 \cdot 1.5H_2O$; [b]a sum of aragonite-K, K_2CO_3, and $K_2CO_3 \cdot 1.5H_2O$; [c]a sum of OM-K1 and OM-K2. Molar contribution (%) of each K species to total K in carbonates as quantified by linear combination fitting (LCF) analysis of the first derivative of K K-edge XANES spectra of the best least square fit ranked after the R-factor (R).
Note 2: The standard errors in the parentheses are for the LCF analysis although the actual uncertainties for the overall XANES-LCF analysis could be lower. We used a residual parameter R-factor ($R = \Sigma(datafit)^2/\Sigma(data)^2$) to evaluate the goodness of fitting, and the best fit was selected based on the R ranking in Athena.
Note 3: In the "sum" panel, K hosted in K_2CO_3 is a sum of K_2CO_3 and $K_2CO_3 \cdot 1.5H_2O$. K hosted in carbonates is a sum of K_2CO_3, $K_2CO_3 \cdot 1.5H_2O$ and aragonite-K. K hosted in organic matrices is a sum of soluble OM-K1 and insoluble OM-K2.

surements of certified references yielded a long-term uncertainty of K isotope analysis by MC-ICP-MS is 0.11‰ (2 S.D., Chen et al., 2019). We use a notation $\Delta^{41}K_{x\text{-}y}$ equal to $\delta^{41}K_x$-$\delta^{41}K_y$ to express K isotope fractionation between the components x and y. We note that confidence intervals (95% c.i.) were used to reflect statistical clarity:

$$95\%\ \text{c.i.}(‰) = t_{n-1} \times \frac{S.D.}{\sqrt{n}}, \tag{2}$$

where S.D. represents the standard deviation over analytical sessions (n times), and t_{n-1} denotes the student's law factor with $(n-1)$ degrees of freedom at a 95% confidence level. Estimated uncertainties on K isotope measurement and XANES-LCF were propagated:

$$\Delta E = \sqrt{(c_1 \Delta W_1)^2 + (c_2 \Delta W_2)^2 + \cdots + (c_n \Delta W_n)^2}, \tag{3}$$

where ΔE is an absolute error, c is a multiplicative factor, and W is additive function inputs.

3. Results

3.1. Elemental and isotopic composition

The geochemical composition of *Porites* corals is summarized in Table 2 and displayed in Figs. 1 and S3-S4. The K concentration in coral skeletons ranges from 3.1 to 170.3 mg/kg (colony C, low zooxanthellae-density) and 32.1 to 396.9 mg/kg (colony B, high zooxanthellae-density), without temperature dependence (Fig. 1a). To assess the degree of K incorporation from seawater in corals, the partitioning coefficient is defined:

$$K_D^{K/Ca} = \left(\frac{K}{Ca}\right)_{Coral} / \left(\frac{K}{Ca}\right)_{Seawater}, \tag{4}$$

where (K/Ca) represents the molar ratios of K to Ca (Table 2). The partitioning coefficient of K in corals does not correlate with temperature (Fig. 2a). The calcification rate of corals ranges from 0.7 to 14.1 mg/day (colony C) and 7.4 to 19.4 mg/day (colony B), and coral calcification rate positively correlates with the K partitioning coefficient ($R^2 = 0.18$, $p<0.05$, Fig. 2b). The calcification rate of colony B is overall higher than that of colony C, in line with a higher zooxanthellae density in colony B (Materials and Methods). We identified a positive relationship between temperature and coral calcification rate (Fig. 1b), and this correlation is marked in colony C ($R^2 = 0.81$, $p<0.001$) relative to colony B ($R^2 = 0.05$, $p<0.5$) (Fig. 2c). Coral $\delta^{41}K$ range from -1.88 ± 0.19 to 0.69 ± 0.07‰ (colony C) and -0.83 ± 0.18 to 0.79 ± 0.07‰ (colony B). In addition to cultured corals, field-collected *Porites* coral (CR-FL-Ps) exhibits the bulk $\delta^{41}K$ value of 0.37 ± 0.10‰, which is higher than that of skeletal organic matrices (-1.80 ± 0.11‰). It seems that intracrystalline organic matter of *Porites* corals preferentially has isotopically light K. Skeletal $\delta^{41}K$ values are higher than or close to seawater $\delta^{41}K$ at 20-25 °C, and lower than seawater $\delta^{41}K$ at 27-29 °C (Fig. 1c). Skeletal $\delta^{41}K$ negatively correlates with seawater temperature (Fig. 1c). The relationships can be characterized by logarithmic functions using all the $\delta^{41}K$ values (Fig. 3a) of samples in different temperature treatments ($R^2 = 0.95$, colony C, and 0.60 for colony B, $p<0.001$). As for the comparison between coral calcification rate and $\delta^{41}K_{Coral}$, we find a negative linear relationship in colony C ($R^2 = 0.86$, $p<0.001$). However, this correlation is not statistically distinguishable for colony B (Fig. 3b).

3.2. XANES and skeletal K speciation

We have identified and quantified skeletal K phases using K *K*-edge XANES, resulting from the contribution associated with the atomic structural arrangement around K and electronic contribution from the interaction with other atoms surrounding K (Fig. 4). The change in the K phase can be visually derived based on the magnitudes of spectral peaks at ~3610-3615 eV (brown bar) and valleys at ~3618-3622 eV (yellow bar) (Fig. 4). The former corresponds to the spectral feature of K_2CO_3 phases (K_2CO_3 and $K_2CO_3 \cdot 1.5H_2O$), and the latter shows the feature of organic-K speciation (soluble OM-K1 and insoluble OM-K2) (Fig. 4). Based on XANES-LCF results (Table 1 and Figs. 4 and S5), K_2CO_3 and $K_2CO_3 \cdot 1.5H_2O$, K-bearing aragonite, and skeletal organic matrices (soluble OM-K1 and insoluble OM-K2) provide the best fit. The fraction of K_2CO_3 ranges from 0 to 5.8 ± 3.7% (colony C) and 0 to 9.6 ± 4.0% (colony B), and the fraction of $K_2CO_3 \cdot 1.5H_2O$ ranges from 7.3 ± 2.7 to 26.4 ± 6.7% (colony C) and 10.4 ± 4.0 to 31.7 ± 4.3% (colony B). Thus, the percent of K hosted in K_2CO_3

Table 2
Elemental and isotopic data for cultured scleractinian corals from this study.

Sample ID		Total K (mg/kg)	Target T (°C)	Actual T (°C)	Growth rate (%)	Calcification rate (mg/d)	$10^3K_D^{K/Ca}$	$\delta^{41}K$ (‰)	95% C.I. (‰)	1S.D. (‰)	N
Scleractinian *Porites* coral	C-1	59.2	29.0	29.2	32.3	13.9	0.21	−1.88	0.19	0.12	6
Colony C	C-2	36.3	29.0	29.2	28.4	14.1	0.10	−1.59	0.19	0.15	6
(low zooxanthellae-density)	C-3	53.2	29.0	29.2	27.7	12.3	0.13	−1.56	0.26	0.17	9
	C-4	3.1	27.0	27.0	12.1	8.5	0.01	−0.83	0.18	0.17	7
	C-5	51.3	27.0	27.0	23.6	9.6	0.13	−0.33	0.08	0.11	7
	C-6	78.7	27.0	27.0	32.2	8.5	0.11	−0.25	0.05	0.04	5
	C-7	47.8	25.0	25.1	22.8	9.7	0.10	0.04	0.11	0.10	7
	C-8	44.2	25.0	25.1	13.7	7.0	0.09	−0.12	0.08	0.06	5
	C-9	52.2	25.0	25.1	9.8	5.0	0.09	0.24	0.11	0.11	7
	C-10	20.3	25.0	25.1	17.0	7.9	0.06	0.19	0.03	0.03	7
	C-11	12.3	25.0	25.1	19.6	10.1	0.07	n.d.	n.d.	n.d.	n.d.
	C-12	69.4	25.0	25.1	10.2	5.5	0.12	0.14	0.10	0.08	5
	C-13	10.6	23.0	23.2	8.2	3.9	0.04	0.43	0.06	0.06	6
	C-13*	120.0	23.0	23.2	8.2	3.9	0.17	n.d.	n.d.	n.d.	n.d.
	C-14	7.2	23.0	23.2	11.2	4.9	0.02	n.d.	n.d.	n.d.	n.d.
	C-14*	170.3	23.0	23.2	11.2	4.9	0.16	0.61	0.09	0.07	7
	C-15	99.3	23.0	23.2	11.2	6.3	0.16	0.34	0.05	0.04	6
	C-15*	135.0	23.0	23.2	11.2	6.3	0.16	n.d.	n.d.	n.d.	n.d.
	C-17	101.8	20.0	19.9	6.1	4.0	0.17	0.69	0.07	0.06	7
	C-18	94.6	20.0	19.9	2.1	0.7	0.14	n.d.	n.d.	n.d.	n.d.
Scleractinian Porites coral	B-1	32.1	29.0	29.2	48.1	18.1	0.11	−0.34	0.05	0.04	5
Colony B	B-2	97.5	29.0	29.2	34.9	13.0	0.12	−0.83	0.18	0.12	7
(high zooxanthellae-density)	B-3	86	29.0	29.2	49.6	16.3	0.15	n.d.	n.d.	n.d.	n.d.
	B-4	122.1	27.0	27.0	31.9	13.6	0.25	−0.20	0.07	0.06	5
	B-5	68.3	27.0	27.0	22.9	7.4	0.14	−0.73	0.11	0.09	5
	B-6	80.8	27.0	27.0	37.9	10.8	0.18	0.44	0.08	0.07	7
	B-8	108.2	27.0	27.0	29.9	10.9	0.18	0.16	0.05	0.04	6
	B-9	128.0	27.0	27.0	27.0	10.3	0.16	0.39	0.03	0.03	7
	B-10	219.1	25.0	25.1	45.4	19.4	0.27	0.50	0.10	0.08	6
	B-11	396.9	25.0	25.1	41.4	13.8	0.56	n.d.	n.d.	n.d.	n.d.
	B-12	123.0	25.0	25.1	45.5	17.5	0.16	0.39	0.03	0.03	5
	B-13	47.7	23.0	23.2	39.2	15.5	0.09	n.d.	n.d.	n.d.	n.d.
	B-13*	117.2	23.0	23.2	39.2	15.5	0.17	n.d.	n.d.	n.d.	n.d.
	B-14	198.9	23.0	23.2	27.0	12.2	0.33	0.63	0.08	0.07	6
	B-14*	149.2	23.0	23.2	27.0	12.2	0.21	0.61	0.09	0.07	5
	B-15	120.2	23.0	23.2	39.8	13.3	0.14	0.65	0.13	0.10	7
	B-15*	165.3	23.0	23.2	39.8	13.3	0.20	n.d.	n.d.	n.d.	n.d.
	B-16	165.3	20.0	19.9	24.6	9.6	0.21	0.79	0.07	0.06	5
	B-17	204.9	20.0	19.9	26.9	11.6	0.15	0.60	0.03	0.03	6
	B-18	87.8	20.0	19.9	26.9	9.4	0.18	0.66	0.10	0.08	5
Bulk *Porites*	CR-FL-Ps	193.3	n.d.	n.d.	n.d.	n.d.	0.21	0.37	0.10	0.08	5
Organic matrix	CR-FL-Ps*	-	-	-	-	-	-	-1.80	0.11	0.10	5

Note: *denote the re-sampling of powders of new slabs from different parts of coral skeletons; n.d. denotes "not determined"; N: total analytical cycles for each sample during MC-ICP-MS isotope measurement. $K_D^{K/Ca}$ represents the coral-seawater partitioning coefficient of K (i.e., $K_D^{K/Ca}=(K/Ca)_{Coral}/(K/Ca)_{Sea}$).

phases ranges from 7.3±2.7 to 31.8±7.3% (colony C) and 20.0±5.7 to 40.6±5.9% (colony B). The proportion of aragonite-K ranges from about 0 to 15.6±6.3% (colony C) and ~0 to 19.7±3.8% (colony B). The percent of K hosted in carbonate phases (a sum of K_2CO_3, $K_2CO_3{\cdot}1.5H_2O$, and aragonite-K) ranges from 7.3±2.7 to 41.9±8.5% (colony C) and 20.0±13.1 to 60.3±7.1% (colony B). The OM-K1 fraction ranges from 0 to 91.5±5.6% (colony C) and 34.3±6.6 to 50.5±9.4% (colony B), and the OM-K2 proportion ranged from ~0 to 58.0±4.9% (colony C) and 5.4±2.2 to 31.2±4.8% (colony B). In sum, the proportion of K in organic matrices ranges from 58.0±2.9 to 92.5±5.7% of colony C and 39.7±7.0 to 79.3±13.4% of colony B.

4. Discussion

The K isotope fractionation between cultured corals and seawater shows large variations in different temperature settings. We assess potential mechanisms of K incorporation in coral skeletons before addressing dominant causes of observed K isotope fractionation.

4.1. Mechanisms of K incorporation in coral skeletons

Based on XANES-LCF (Fig. 4), we determined the presence of K in both skeletal organic matrices and carbonate phases of variable proportions for *Porites* corals (Table 1). This K phase partitioning in biogenic carbonates is expected because of the importance of so-called "vital effects"– biologically mediated elemental distribution during biomineralization (Sinclair et al., 2006; Li et al., 2021b). Similar to the case of K, the association of Na, P, and Zn to coral skeletal organic matrices was confirmed by chemical extraction (M. Chen et al., 2019; Zhao et al., 2021) and XANES studies (Yoshimura et al., 2017). Therefore, we consider that the partitioning of the elements into carbonate and organic phases in coral skeletons is common. We then evaluate the mechanisms of K incorporation.

First, we assess the occurrence of organic-K phases in cleaned coral skeletons. Although oxidative reagents can react with animal soft tissues, organic matrices in between $CaCO_3$ laminates where calcification occurs can be largely preserved (Ingalls et al., 2003). Hence, organic-K phases (XANES) likely exist as intracrystalline organics. It is known that coral calcification requires the functioning of skeletal organic matter as the substrate for $CaCO_3$ nucleation affecting the composition and morphology of aragonite (Dauphin et al., 2006; Falini et al., 2015; Von Euw et al., 2017). We suggest that K^+ in coral skeletons potentially situates in skeletal organic substrate involved in biomineralization. It is supported by the fact that the functioning of Na^+/K^+-ATPase promotes the introduction of Ca into calcifying spaces, and Na^+/K^+-ATPase consumes energy de-

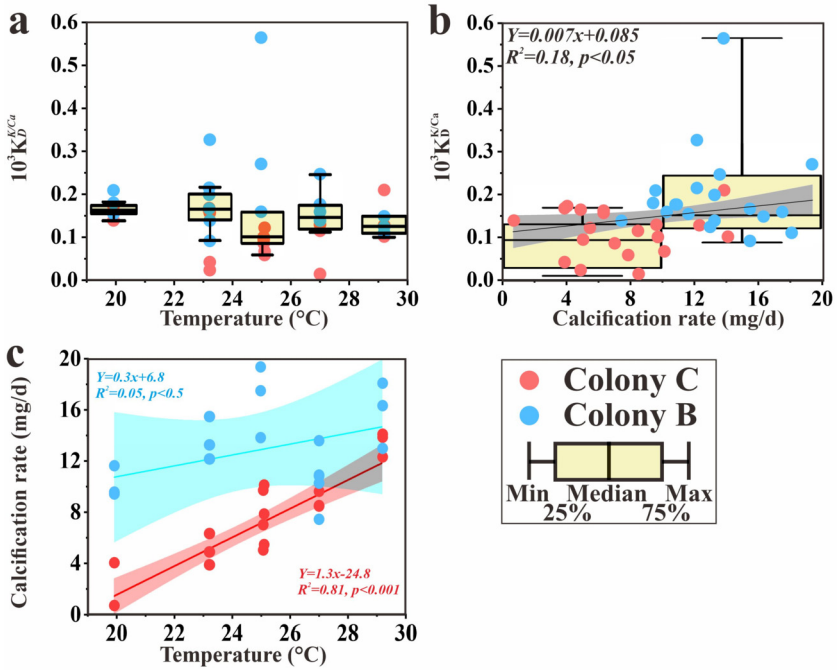

Fig. 2. Changes in skeletal K chemistry and growth of cultured corals. (a) Temperature versus $10^3K_D^{K/Ca}$ ($K_D^{K/Ca}=(K/Ca)_{Coral}/(K/Ca)_{Sea}$). (b) coral calcification rate versus $10^3K_D^{K/Ca}$. The black line shows the linear fitting of all the data. (c) Calcification rate as a function of seawater temperature. The cyan and red lines represent linear fittings for colonies B (high zooxanthellae-density) and C (low zooxanthellae-density), respectively. Shaded regions (black, cyan, and red) represent the 95% confidence bands. In the plots (a and b), skeletal data at each temperature interval are covered using the box chart.

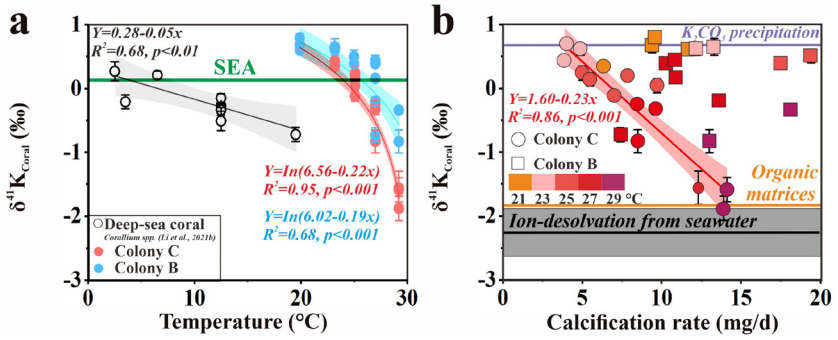

Fig. 3. Variations in skeletal $\delta^{41}K_{Coral}$ values of cultured corals. (a) temperature (actual temperature) versus $\delta^{41}K_{Coral}$. In plot (a), the black, cyan, and red lines represent the linear fittings (logarithmic) for deep-sea coral (*Corallium spp.*) reported in Li et al. (2021b), colonies B (high zooxanthellae-density) and C (low zooxanthellae-density) using the data of samples at all temperature, respectively. Shaded regions (black, cyan, and red) show 95% confidence bands. The green line indicates $\delta^{41}K$ of seawater (SEA, ~0.12‰, Hille et al., 2019; Wang et al., 2020). (b) Calcification rate versus $\delta^{41}K_{Coral}$. The $\delta^{41}K_{Coral}$ range is constrained by K isotope fractionation from seawater during K^+ desolvation (gray bar, a kinetic isotope mechanism, Hofmann et al., 2012), $K_2CO_3{\cdot}1.5H_2O$ precipitation at room temperatures (purple line, an equilibrium isotope mechanism, Li et al., 2017), and the isotopic composition of K in extracted skeletal organic matrices from a field-collected coral (orange line, CR-FL-Ps, -1.80±0.11‰). The data of colonies B and C are symbolized using cubes and circles, respectively. In plot (b), the colors from orange to dark red indicate seawater temperature increasing from low (~20 °C) to high (~29 °C).

rived from ATP hydrolysis to export Na^+ via the cell membrane for the import of K^+ (Ip et al., 2015). Hence, seawater-derived K^+ may be added into calcifying spaces by biological processes, and a close association of K^+ with skeletal organic matrices is expected. Based on the results of XANES, skeletal partitioning of K is featured by higher contents of organic-K at higher temperatures (also higher calcification rates, Figs. 2c and 4). A possible explanation of this difference is the promotion of skeletal organic matrices to the development of scleractinian coral skeletons (Reggi et al., 2014). This pattern is consistent with the rhythmic accumulation of K within the skeletons where $CaCO_3$ crystals form rapidly with locally enriched organic matter for shallow-water, reef-building corals, and deep-sea corals (Meibom et al., 2008; Mitsuguchi and Kawakami, 2012).

Next, we address the occurrence of carbonate-bound K phases during coral calcification. During biomineralization, ions in calcifying fluids may be fixed within carbonate structures during the propagation of skeletal materials and subsequent bond formation in the crystal. A growing body of evidence suggests that metal cations may be incorporated in biogenic carbonates as a function of seawater chemistry and other environmental factors including temperature and pH (Gaetani et al., 2011; Montagna et al., 2014; Wall et al., 2019). The fundamental assumption of this interpretation is $CaCO_3$ precipitation by marine calcifiers may be analogous to its inorganic precipitation in (semi)-enclosed environments that are modified in their elemental and carbonate chemistry with respect to surrounding seawater. Five potential processes are listed below and evaluated to explain ion incorporation into carbonates and understand how K occurs in coral skeletons (White, 1977; Ishikawa and Ichikuni, 1984; Okumura and Kitano, 1986; Mitsuguchi and Kawakami, 2012; Yoshimura et al., 2017; Li et al., 2021b).

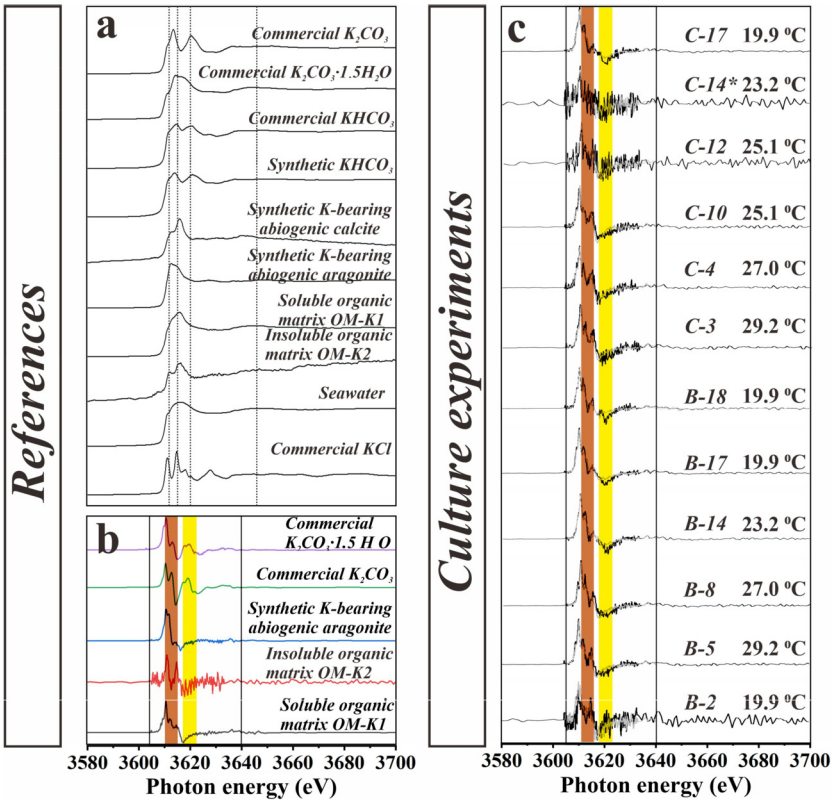

Fig. 4. Skeletal K *K*-edge XANES spectra and XANES-LCF analysis in cultured corals. (a) A spectral compilation of possible K phases in coral skeletons (some data come from Li et al., 2020). (b) The first derivative of the spectra of major K phases in coral skeletons using Athena software (Ravel and Newville, 2005) (XANES-LCF in a range from 3605 to 3640 eV). (c) The result of XANES-LCF with the first derivative of spectra. The black and grey lines represent the original spectra and fitting curves, and the box framework shows the fitting range. The brown and yellow bars denote major spectral variations, indicating the increase in the K fractions hosted in organic matrices and decrease in the K fractions hosted in K_2CO_3 (K_2CO_3 and $K_2CO_3 \cdot 1.5H_2O$) with increasing temperature for two colonies.

1) $2Ca^{2+} = 2K^+ + O$ (vacancy) (*charge compensation by a structural defect*)
2) $Ca^{2+} + CO_3^{2-} = K^+ + HCO_3^-$ (*charge balance by coupled substitution with a bicarbonate*)
3) $Ca^{2+} + CO_3^{2-} = K^+ + Cl^-$ (*charge compensation by coupled substitution by a halite as Cl^-*)
4) $2Ca^{2+} = K^+ + Al^{3+}$ (*charge compensation by coupled substitution of trivalent ions as Al^{3+}*)
5) Seawater inclusion (*seawater trapping in calcification sites via intercellular junctions*)

The XANES-LCF results indicate that the first process is probably the dominant control of K incorporation into carbonate phases due to the presence of K_2CO_3 and aragonite-K (Table 1). As for the presence of poorly crystalline K_2CO_3 phases (XANES-based K_2CO_3 and $K_2CO_3 \cdot 1.5H_2O$, a possible explanation is that K is sequestrated into poorly ordered $CaCO_3$, such as amorphous calcium carbonates (ACC). Supportively, amorphous $CaCO_3$ (e.g., Ca-ACC and Mg-ACC in a short-range order, Mergelsberg et al., 2020) has been recognized as the precursor material in biomineralization for various calcifying organisms, including *Porites* coral (Von Euw et al., 2017). The importance of trace and major element incorporation into ACC for various kinds of marine organisms that generate biominerals has been highlighted by Evans et al. (2020). The nano-sized amorphous $CaCO_3$ deposits on the organic substrate, where they can remain stable and may even exist for years prior to $CaCO_3$ crystallization (Stan et al., 2017; Montagna et al., 2014; Sun et al., 2020). This process potentially inhibits the transformation of amorphous intermediate phases to more crystalline aragonite skeletons. As for the presence of aragonite-K, the XANES data are consistent with the results of carbonate synthesis experiments by Okumura and Kitano (1986), suggesting that alkali metal cations (e.g., Li^+, Na^+, and K^+) prefer to substitute for nine-coordinated Ca^{2+} within aragonite. The second process is less likely because the spectral features of $KHCO_3$ are not found in XANES and the addition of $KHCO_3$ spectra reduces the fitting goodness (R factor) (Fig. 4). The third process was advocated in early studies, where nano-sized halite was found at the grain boundary and domains of coral skeletons (Motai et al., 2016), and the occurrence of KCl in skeletons was deduced based on K XANES for *Porites lutea*, *P. lobata*, *Pavona gigantea*, and *Montastraea annularis* (Pingitore et al., 2001). However, it is unlikely a case in this study given the disappearance of XANES features of solid-state KCl (Fig. 4). The fourth process - charge compensation by coupled substitution of trivalent ions as Al^{3+} could be negligible if any, due to low Al/K ratios (Table S3). The last process - seawater inclusion is also unlikely since we did not find seawater K signal, in line with XANES survey of biogenic carbonates (Li et al., 2021b).

4.2. Physiological modulation on K isotope fractionation

Here, we examine the control of physiological modulation (or the vital effect) linked with environmental factors such as the effect of temperature on the K isotope fractionation in corals during uptake from seawater. Much of the current understanding of the element and its isotope partitioning during biomineralization of marine organisms comes from the comparison of skeletal geochemical features to abiotic carbonates formed in chemical equilibrium (Gaetani et al., 2011; Saenger and Wang, 2014; Inoue et al., 2015; Evans et al., 2020). Coral calcification can be considered as a semi-closed system with seawater supply through paracellular transport (e.g., Falini et al., 2015; Gagnon et al., 2012).

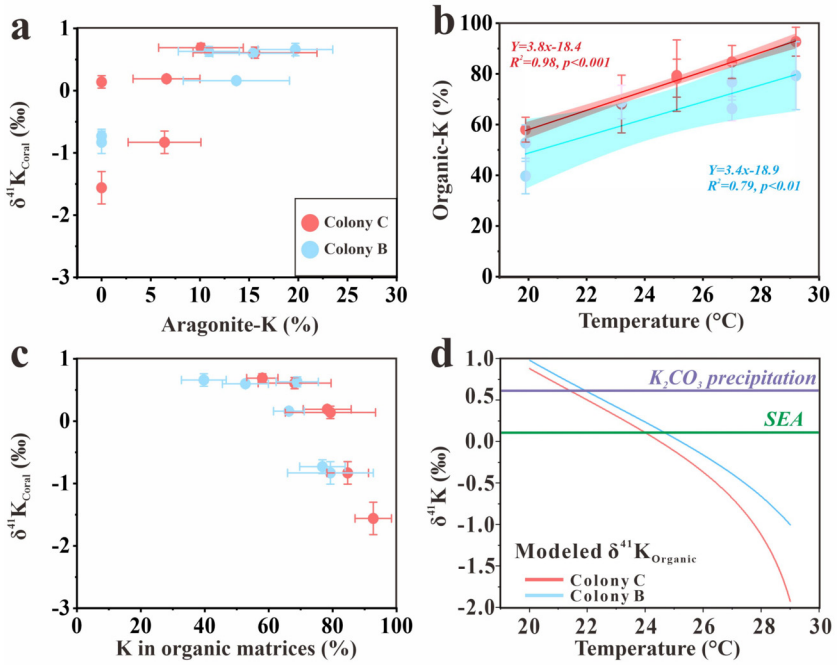

Fig. 5. Skeletal K speciation and K isotope composition in cultured corals. (a) $\delta^{41}K_{Coral}$ versus XANES-based aragonite-K fraction. (b) Seawater temperature versus K in organic matrices (a sum of soluble OM-K1 and insoluble OM-K2). (c) K in organic matrices versus $\delta^{41}K_{Coral}$. (d) Modeled isotopic composition of skeletal organic matrices ($\delta^{41}K_{Organic}$) as a function of temperature. The error bars are plotted using the uncertainties of XANES-LCF from Athena software and MC-ICP-MS isotope analysis. The cyan and red lines represent the linear fittings for colonies B (high zooxanthellae-density) and C (low zooxanthellae-density), respectively. In plot (b), the shaded areas show 95% confidence bands. In plot (d), the $\delta^{41}K$ values of $K_2CO_3{\cdot}1.5H_2O$ precipitated from seawater (purple line, equilibrium mechanism, Li et al., 2017) and modern seawater (green line, Hille et al., 2019; Wang et al., 2020) are provided for comparison.

Hence, seawater probably serves as the basic component of calcifying fluids. Hence, biogenic carbonates may precipitate in isotopic equilibria with seawater. There are two supportive features of cultured *Porites* corals. First, we determine a statistically significant correlation between temperature and $\delta^{41}K_{Coral}$, and this empirical logarithmic pattern is applicable for both colonies (Fig. 3a). Second, the most positive $\delta^{41}K_{Coral}$ value may be constrained by an equilibrium K isotope fractionation of ~0.50‰ between $K_2CO_3{\cdot}1.5H_2O$ and dissolved K^+ in surrounding liquid medium at 25 °C (Li et al., 2017) (Fig. 3b). The presence of K_2CO_3 phases (K_2CO_3 and $K_2CO_3{\cdot}1.5\ H_2O$) in coral skeletons is determined by XANES (Table 1). The occurrence of K linked with aragonite (aragonite-K) is identified by XANES as well, but the degree and magnitude of corresponding isotopic fractionation remain unclear. If the kinetic isotope effect matters, this mechanism may partially explain the low $\delta^{41}K_{Coral}$ from −1 to −2‰ (Fig. 1c). For example, Nielsen et al. (2012) proposed an ion-by-ion growth theory of the kinetic isotope fractionation during carbonate crystallization, promoting the incorporation of light Ca isotopes in the lattice. Alternatively, a kinetic isotope fractionation factor ($\alpha_{Carbonate\text{-}Sea}$) of 0.9976±0.0004 (between carbonates and seawater) was estimated for K^+ desolvation from water during carbonate precipitation using molecular dynamics simulation (Hofmann et al., 2012), which could explain the lowest $\delta^{41}K_{Coral}$ value (Fig. 3b). In contrast, we find a positive relationship between XANES-based aragonite-K proportion and $\delta^{41}K_{Coral}$ value (Fig. 5a), implying preferential incorporation of isotopically heavy K into aragonitic skeletons, presumably following an equilibrium path. However, if equilibrium isotope fractionation is the only cause of isotopic fractionation in corals, then we would expect a decrease in measured K isotope fractionation (i.e., $\triangle^{41}K_{Sea\text{-}Coral}$) as temperature increases (Schauble, 2004), which is opposite to the experiment results in a temperature range of 25 to 29 °C (Fig. 1c). Moreover, natural deep-sea coral (*Corallium spp.*) exhibits an increase in the net K isotope fractionation ($\triangle^{41}K_{Sea\text{-}Coral}$) with increasing temperature (Li et al., 2021b, Fig. 3a). Therefore, physiological controls may play a role in balancing the K isotope effect in corals.

Here, we suggest that there may be a temperature-sensitive physiological modulation of skeletal K phases responsible for the observed isotopic fractionation patterns in corals, which is supported by the following K isotope and XANES results. The relative proportion of K associated with organic matrices (~40 to 90%) gradually exceeds that of carbonate-K (7 to 60%) as temperature increases (Fig. 5b), accompanied by reversed $\Delta^{41}K_{Coral\text{-}Sea}$ from positive offsets at 20-25 °C to negative offsets at 27-29 °C (Fig. 1c). Hence, we infer that organic-K phases have lower $\delta^{41}K$ to counter the imprint of carbonate-K, which is isotopically heavier. It may be ascribed to biologically mediated enrichment of isotopically light K in skeletal organic matrices, and the fraction of organic-K (^{39}K rich) increases with temperature (Table 1). The affinity of ^{39}K to skeletal organic matrices can be supported by K isotope fractionation of −1.92‰ between chemically extracted organic matrices from a natural *Porites* coral (CR-FL-Ps) and seawater (0.12‰, Hille et al., 2019; Wang et al., 2020) (Table 2), which might be the case for cultured *Porites* corals. We also identified a negative correlation between the K fraction hosted in skeletal organic matrices (a sum of insoluble OM-K1 and soluble OM-K2 from XANES) and $\delta^{41}K_{Coral}$ (Fig. 5c). The correlation between organic-K and $\delta^{41}K_{Coral}$ demonstrates relatively low $\delta^{41}K$ values of intracrystalline organic matrices ($\delta^{41}K_{Organic}$) compared to those in carbonate-K (K_2CO_3, $K_2CO_3{\cdot}1.5H_2O$, and aragonite-K). However, we also have concerns on the reliability of $\delta^{41}K_{Organic}$ values provided by the extracted organic matrices of a field-collected *Porites* coral, as it can be different from cultured corals in their geochemical composition and biological properties. Finally, the isotopic fractionation during chemical extraction cannot be excluded, which may induce a very negative isotopic value ($\delta^{41}K_{Organic}$ of −1.80‰, Fig. 3b). Therefore, we provide an estimation of $\delta^{41}K_{Organic}$ in cultured corals combining XANES and isotopic data.

We suggest that skeletal $\delta^{41}K_{Coral}$ reflects a sum of relative contributions from carbonate-K and organic-K phases, which can be expressed as below. We note that uncertainties in XANES-LCF may cause bias, and model analysis only attributes skeletal $\delta^{41}K$ variation to phase partitioning, which may be oversimplified.

$$\delta^{41}K_{Coral} = \delta^{41}K_{Carbonate} \times f_{Carbonate} + \delta^{41}K_{Organic} \times f_{Organic}, \quad (5)$$

where $f_{Carbonate}$ and $f_{Organic}$ represent the relative proportion of carbonate-K and organic-K determined by XANE-LCF, respectively, and a sum of $f_{Carbonate}$ and $f_{Organic}$ equals to 100%. From experimental data, $\delta^{41}K_{Coral}$, $f_{Carbonate}$ and $f_{Organic}$ are the functions (F) of temperature (T) (the formulas in Fig. 3a and 5b). Equation (5) can be converted to the following form:

$$F\left(\delta^{41}K_{Coral}\right) = \delta^{41}K_{Carbonate} \times F(f_{Carbonate}) + \delta^{41}K_{Organic} \times F(f_{Organic}), \quad (6)$$

$$F\left(\delta^{41}K_{Coral},\ \text{Colony C}\right) = \text{Ln}(6.56 - 0.22T)\ (‰);$$

$$F\left(\delta^{41}K_{Coral},\ \text{Colony B}\right) = \text{Ln}(6.02 - 0.19T)\ (‰) \quad (7)$$

$$F(f_{Organic},\ \text{Colony C}) = (3.8T - 18.4)\ (\%);$$

$$F(f_{Organic},\ \text{Colony B}) = (3.4T - 18.9)\ (\%) \quad (8)$$

Assuming that $\delta^{41}K_{Carbonate}$ values of K_2CO_3, $K_2CO_3 \cdot 1.5H_2O$, and aragonite-K are similar to that of $K_2CO_3 \cdot 1.5H_2O$ formed in isotope equilibria ($\triangle^{41}K_{Carbonate\text{-}Sea}$ of 0.50‰, $\delta^{41}K_{Carbonate}$=0.62‰, Li et al., 2017), we can estimate $\delta^{41}K_{Organic}$ with the following equation:

$$\delta^{41}K_{Organic} = \left[F\left(\delta^{41}K_{Coral}\right) - \delta^{41}K_{Carbonate} \times F(f_{Carbonate})\right] / F(f_{Organic}), \quad (9)$$

Combined with equations (6), (7), and (8), the equation (9) can be converted to another form:

$$\delta^{41}K_{Organic}\ (\text{Colony C}) = \left[100\text{Ln}(6.6 - 0.2T) - 73.4 + 2.4T\right] / (3.8T - 18.4)\ (‰),$$

$$\delta^{41}K_{Organic}\ (\text{Colony B}) = \left[100\text{Ln}(6.0 - 0.2T) - 73.7 + 2.1T\right] / (3.4T - 18.9)\ (‰), \quad (10)$$

Temperature-dependent $\delta^{41}K_{Organic}$ (equation (10)) is derived from experiment correlation between $\delta^{41}K_{Coral}$ and K speciation with seawater temperature. It is a tentative estimation because of large variations in $\delta^{41}K_{Coral}$ at the same temperature (Fig. 1c) and absolute errors of the XANES-LCF method are ~5 to 10% in general, thus more work on $\delta^{41}K_{Organic}$ is required.

We note that the temperature dependence of $\delta^{41}K_{Coral}$ and $f_{Organic}$ (or $f_{Carbonate}$) for colonies B and C are slightly different (Figs. 3a and 5b). Therefore, $\delta^{41}K_{Organic}$ of the two colonies is estimated separately. Modeled $\delta^{41}K_{Organic}$ as a function of temperature is depicted in Fig. 5d. Interestingly, estimated $\delta^{41}K_{Organic}$ changes from positive (20-24 °C) to negative (24-29 °C) values as temperature raises. This may be due to changes in the metabolic pathway in corals (or zooxanthellae) or changing the K uptake rate by corals in response to temperature variation. In most cases (except for 20-21 °C), modeled $\delta^{41}K_{Organic}$ is lower than the expected $\delta^{41}K_{K2CO3}$ of 0.62‰. In the temperature range of 20-24 °C, $\delta^{41}K_{Organic}$ is more positive than $\delta^{41}K_{Sea}$ according to a two-endmember mixing model (Fig. 5d). The preferential uptake of ^{41}K by marine organisms has also been reported for field-collected algae and sea clams, which was explained by the preferential removal of ^{39}K from cells (Li, 2017). At the temperature of 24-29 °C, ^{39}K affinity to organic matter is prominent. There is no robust interpretation of ^{39}K in organic-K, and we propose some possible mechanisms for coral uptake of ^{39}K. K^+-specific channels are proteins enabling K permeation across cellular membranes. For K^+ transport, Bucher et al. (2010) predicted an increase in the coordination number of K^+ (N of 6.2–6.6) and elongation of K-O bonds (~2.68–2.89 Å) in K channels. Thus, weaker K-O bonds are formed and lighter K can be linked to organic matrices according to the stable isotope theory (Schauble, 2004).

One important question is why marked differences exist in the temperature dependence of $\delta^{41}K_{Coral}$ for the deep-sea coral (*Corallium spp.*, Li et al., 2021b) and *Porites* colonies B (high zooxanthellae-density) and C (low zooxanthellae-density) (Fig. 3a). The difference between deep-sea corals and cultured colonies could be attributed to a species-specific feature during phase partitioning. For example, the calcite-K phase can only be found by XANES data of deep-sea corals examined in Li et al. (2021b). For inter-colony differences (B and C), we note that the K partitioning within coral skeletons of two colonies is different at the same temperature (more organic-K fraction and lower $\delta^{41}K_{Coral}$ in colony C), which may be physiologically regulated. For *Porites* corals, calcification is largely modulated by the mutualism between coral and endosymbiotic zooxanthellae (Knowlton and Rohwer, 2003; McCulloch et al., 2017). Therefore, biologically mediated elemental and isotopic partitioning (i.e., the vital effect) in corals depends on zooxanthellae density. The higher zooxanthellae density in colony B relative to colony C might be the cause of differences in K speciation and isotope composition of *Porites* corals in the same culturing conditions.

Finally, we assess the impact of biologically mediated calcification, which is complicated by temperature interference due to the positive correlation between the two factors (Fig. 2c). However, the weak dependence of the calcification rate of colony B on temperature offers important insights. We identified a negative relationship between the calcification rate and $\delta^{41}K_{Coral}$ in coral colony C, which may be attributed to the direct correspondence of temperature and calcification kinetics (Fig. 3b). Given the enhancement in metabolic activity (temperature related), more energy may be used by organisms to produce organic matter facilitating skeleton growth (Dauphin et al., 2006). Hence, more organic-K phases with lower $\delta^{41}K$ are generated with higher calcification rates at higher-temperature. This pattern was not distinguished for the dataset of colony B with higher calcification rates, showing relatively poor correlations between temperature and calcification rate (Fig. 2c). The higher density of zooxanthellae probably promotes photosynthesis and generates more energy for coral growth but may reduce the linkage between calcification rate with temperature and organic matter production. Hence, we infer the variation in coral skeletal $\delta^{41}K$ cannot be attributed to a simple growth-rate effect. Likewise, the absence of growth-rate related kinetic controls on coral $\delta^{18}O$, $\delta^{44}Ca$, and Sr/Ca in cultured *Porites* corals were reported (Suzuki et al., 2005; Hayashi et al., 2013; Inoue et al., 2015). It is possible that the temperature and calcification correspondence and growth-rate controls on coral isotopic composition start to diminish when the density of zooxanthellae in corals exceeds a threshold. Hence, future studies could include expanding coral sets with wide variability in zooxanthellae density and seawater temperature for *Porites* and other scleractinians.

5. Summary and implications

Our study investigated the K speciation and isotope composition in *Porites* corals cultured at a range of temperatures using synchrotron-based spectroscopic and high-resolution isotopic measurements. We conclude that the incorporation of K into scleractinian coral skeletons (*Porites australiensis*) is potentially driven by the altervalent substitution of K for Ca in carbonate phases and K incorporation in skeletal organic matrices. The relative proportion

of K hosted in carbonate phases to that of K associated with intracrystalline organic matrices is affected by temperature-sensitive physiological modulation. The inter-colony difference in the K fraction in skeletal organic matrices may be ascribed to a link between the zooxanthellae density and the biological activity of zooxanthellae in *Porites* corals. This study experimentally constrains the K isotope fractionation factors between scleractinian coral skeletons and seawater. The K isotope composition in coral skeletons became lighter with increasing temperature, likely reflecting changes in the comparative contribution of isotopically lighter K in intracrystalline organic matrices and isotopically heavier carbonate-bearing K, including K_2CO_3, $K_2CO_3 \cdot 1.5H_2O$, and aragonite-K. The data of this study emphasizes a phase-dependent fractionation process rather than a constant isotope fractionation factor of K between coral skeleton and seawater. On a positive note, coral K phases and $\delta^{41}K$ add to the understanding of the link between coral growth and biomineralization. We suggest that a combination of isotope and XANES-based phase analyses of biogenic carbonates offers a better understanding of the record of seawater chemistry and biological modulation. However, research on fossil carbonates with organic matrix degradation may be difficult. In sum, the variability in isotope fractionation between calcified skeletons and surrounding seawater needs additional attention on the control of temperature on seawater isotopic information archived in marine biogenic carbonates. We infer that a similar issue probably exists for other taxa of calcifying organisms and calcified marine sediments due to the redistribution of K into various skeletal phases dependent on multiple environmental factors. We note that future applications of using coral records to reconstruct seawater $\delta^{41}K$ signals have limitations due to temperature and physiological interference. Therefore, future studies on the K isotope fractionation between abiotically formed carbonates and other types of marine calcified organisms as foraminifera and brachiopods with surrounding waters are needed.

CRediT authorship contribution statement

Wenshuai Li: Conceptualization, Data curation, Analysis, Investigation, Methodology, Visualization, Writing - original draft, Writing - review & editing. **Xiao-Ming Liu:** Conceptualization, Funding acquisition, Investigation, Methodology, Validation, Writing - review & editing. **Kun Wang:** Methodology, Writing - review & editing. **Yongfeng Hu:** Methodology, Writing - review & editing. **Atsushi Suzuki:** Methodology, Experiment setup, Writing - review & editing. **Toshihiro Yoshimura:** Methodology, Writing - review & editing.

Declaration of competing interest

The authors declare that they have no known competing financial interests or personal relationships that could have appeared to influence the work reported in this paper.

Acknowledgements

We acknowledge funding support from the NSF Career Award (EAR-1848153) to X.-M. Liu, and the Martin fellowship from the University of North Carolina, Chapel Hill to W.-S. Li. We thank Louis Derry and Andrew Jacobson for editorial handling and four anonymous reviewers whose constructive comments significantly improve the paper. We also thank Peter Swart (University of Miami) for providing a natural *Porites* coral sample. We thank Xikai Wang and Mohsen Shakouri for XANES analysis and discussion. We thank Yasuko Koga and Kazuhiko Sakai of the University of the Ryukyus for coral culture experiments. The XANES data were collected at the Canadian Light Source, with the approval of the CLS Proposal Review Committee (32GU010898). The CLS is supported by the Canada Foundation for Innovation, Natural Sciences and Engineering Research Council of Canada, University of Saskatchewan, Government of Saskatchewan, Western Economic Diversification Canada, National Research Council Canada and Canadian Institutes of Health Research.

Appendix A. Supplementary material

Supplementary material related to this article can be found online at https://doi.org/10.1016/j.epsl.2022.117393.

References

Bruggmann, S., Klaebe, R.M., Paulukat, C., Frei, R., 2019. Heterogeneity and incorporation of chromium isotopes in recent marine molluscs (Mytilus). Geobiology 17 (4), 417–435. https://doi.org/10.1111/gbi.12336.

Bucher, D., Guidoni, L., Carloni, P., Rothlisberger, U., 2010. Coordination numbers of K^+ and Na^+ ions inside the selectivity filter of the KcsA potassium channel: insights from first principles molecular dynamics. Biophys. J. 98 (10), L47–L49. https://doi.org/10.1016/j.bpj.2010.01.064.

Chen, H., Tian, Z., Tuller-Ross, B., Korotev, R.L., Wang, K., 2019. High-precision potassium isotopic analysis by MC-ICP-MS: an inter-laboratory comparison and refined K atomic weight. J. Anal. At. Spectrom. 34, 160–171. https://doi.org/10.1039/c8ja00303c.

Chen, H., Liu, X.M., Wang, K., 2020. Potassium isotope fractionation during chemical weathering of basalts. Earth Planet. Sci. Lett. 539, 116192. https://doi.org/10.1016/j.epsl.2020.116192.

Chen, M., Martin, P., Goodkin, N.F., Tanzil, J., Murty, S., Wiguna, A.A., 2019. An assessment of P speciation and P: Ca proxy calibration in coral cores from Singapore and Bali. Geochim. Cosmochim. Acta 267, 113–123. https://doi.org/10.1016/j.gca.2019.09.024.

Dauphin, Y., Cuif, J.P., Massard, P., 2006. Persistent organic components in heated coral aragonitic skeletons-implications for palaeoenvironmental reconstructions. Chem. Geol. 231, 26–37. https://doi.org/10.1016/j.chemgeo.2005.12.010.

Elderfield, H., 2010. Seawater chemistry and climate. Science 327 (5969), 1092–1093. https://doi.org/10.1126/science.1186769.

Evans, D., Gray, W.R., Rae, J.W., Greenop, R., Webb, P.B., Penkman, K., Kröger, R., Allison, N., 2020. Trace and major element incorporation into amorphous calcium carbonate (ACC) precipitated from seawater. Geochim. Cosmochim. Acta 290, 293–311. https://doi.org/10.1016/j.gca.2020.08.034.

Falini, G., Fermani, S., Goffredo, S., 2015. Coral biomineralization: a focus on intraskeletal organic matrix and calcification. Semin. Cell Dev. Biol. 46, 17–26. https://doi.org/10.1016/j.semcdb.2015.09.005.

Frei, R., Paulukat, C., Bruggmann, S., Klaebe, R.M., 2018. A systematic look at chromium isotopes in modern shells–implications for paleo-environmental reconstructions. Biogeosciences 15 (16), 4905–4922. https://doi.org/10.5194/bg-15-4905-2018.

Fujita, K., Hikami, M., Suzuki, A., Kuroyanagi, A., Sakai, K., Kawahata, H., Nojiri, Y., 2011. Effects of ocean acidification on calcification of symbiont-bearing reef foraminifers. Biogeosciences 8, 2089–2098. https://doi.org/10.5194/bg-8-2089-2011.

Gaetani, G.A., Cohen, A.L., Wang, Z., Crusius, J., 2011. Rayleigh-based, multi-element coral thermometry: a biomineralization approach to developing climate proxies. Geochim. Cosmochim. Acta 75, 1920–1932. https://doi.org/10.1016/j.gca.2011.01.010.

Gagnon, A.C., Adkins, J.F., Erez, J., 2012. Seawater transport during coral biomineralization. Earth Planet. Sci. Lett. 329–330, 150–161. https://doi.org/10.1016/j.epsl.2012.03.005.

Gothmann, A.M., Stolarski, J., Adkins, J.F., Higgins, J.A., 2017. A Cenozoic record of seawater Mg isotopes in well-preserved fossil corals. Geology 45, 1039–1042. https://doi.org/10.1130/G39418.1.

Hayashi, E., Suzuki, A., Nakamura, T., Iwase, A., Ishimura, T., Iguchi, A., Sakai, K., Okai, T., Inoue, M., Araoka, S., Murayama, S., Kawahata, H., 2013. Growth-rate influences on coral climate proxies tested by a multiple colony culture experiment. Earth Planet. Sci. Lett. 362, 198–206. https://doi.org/10.1016/j.epsl.2012.11.046.

Hille, M., Hu, Y., Huang, T.Y., Teng, F.Z., 2019. Homogeneous and heavy potassium isotopic composition of global oceans. Sci. Bull. 64, 1740–1742. https://doi.org/10.1016/j.scib.2019.09.024.

Hofmann, A.E., Bourg, I.C., DePaolo, D.J., 2012. Ion desolvation as a mechanism for kinetic isotope fractionation in aqueous systems. Proc. Natl. Acad. Sci. USA 109, 18689–18694. https://doi.org/10.1073/pnas.1208184109.

Huang, T.Y., Teng, F.Z., Rudnick, R.L., Chen, X.Y., Hu, Y., Liu, Y.S., Wu, F.Y., 2020. Heterogeneous potassium isotopic composition of the upper continental crust. Geochim. Cosmochim. Acta 278, 122–136. https://doi.org/10.1016/j.gca.2019.05.022.

Ingalls, A.E., Lee, C., Druffel, E.R.M., 2003. Preservation of organic matter in mound-forming coral skeletons. Geochim. Cosmochim. Acta 67, 2827–2841. https://doi.org/10.1016/S0016-7037(03)00079-6.

Inoue, M., Gussone, N., Koga, Y., Iwase, A., Suzuki, A., Sakai, K., Kawahata, H., 2015. Controlling factors of Ca isotope fractionation in scleractinian corals evaluated by temperature, pH and light controlled culture experiments. Geochim. Cosmochim. Acta 167, 80–92. https://doi.org/10.1016/j.gca.2015.06.009.

Ip, Y.K., Ching, B., Hiong, K.C., Choo, C.Y.L., Boo, M.V., Wong, W.P., Chew, S.F., 2015. Light induces changes in activities of Na^+/K^+-ATPase, H^+/K^+-ATPase and glutamine synthetase in tissues involved directly or indirectly in light-enhanced calcification in the giant clam, Tridacna squamosa. Front. Physiol. 6. https://doi.org/10.3389/fphys.2015.00068.

Ishikawa, M., Ichikuni, M., 1984. Uptake of sodium and potassium by calcite. Chem. Geol. 42 (1–4), 137–146. https://doi.org/10.1016/0009-2541(84)90010-X.

Knowlton, N., Rohwer, F., 2003. Multispecies microbial mutualisms on coral reefs: the host as a habitat. Am. Nat. 162 (S4), S51–S62. https://doi.org/10.1086/378684.

Krief, S., Hendy, E.J., Fine, M., Yam, R., Meibom, A., Foster, G.L., Shemesh, A., 2010. Physiological and isotopic responses of scleractinian corals to ocean acidification. Geochim. Cosmochim. Acta 74, 4988–5001. https://doi.org/10.1016/j.gca.2010.05.023.

Lesser, M.P., Slattery, M., Mobley, C.D., 2018. Biodiversity and functional ecology of mesophotic coral reefs. Annu. Rev. Ecol. Evol. Syst. 49, 49–71. https://doi.org/10.1146/annurev-ecolsys-110617-062423.

Li, S., Li, W., Beard, B.L., Raymo, M.E., Wang, X., Chen, Y., Chen, J., 2019. K isotopes as a tracer for continental weathering and geological K cycling. Proc. Natl. Acad. Sci. USA 116, 8740–8745. https://doi.org/10.1073/pnas.1811282116.

Li, W., 2017. Vital effects of K isotope fractionation in organisms: observations and a hypothesis. Acta Geochim. 36 (3), 374–378. https://doi.org/10.1007/s11631-017-0167-1.

Li, W., Kwon, K.D., Li, S., Beard, B.L., 2017. Potassium isotope fractionation between K-salts and saturated aqueous solutions at room temperature: laboratory experiments and theoretical calculations. Geochim. Cosmochim. Acta 214, 1–13. https://doi.org/10.1016/j.gca.2017.07.037.

Li, W., Liu, X.M., Hu, Y., 2020. Potassium and calcium *K*-edge XANES in chemical compounds and minerals: implications for geological phase identification. Geostand. Geoanal. Res. 44 (4), 805–819. https://doi.org/10.1111/ggr.12351.

Li, W., Liu, X.M., Hu, Y., Teng, F.Z., Hu, Y., 2021a. Potassium isotopic fractionation during clay adsorption. Geochim. Cosmochim. Acta 304, 160–177. https://doi.org/10.1016/j.gca.2021.04.027.

Li, W., Liu, X.M., Wang, K., Fodrie, F.J., Yoshimura, T., Hu, Y.F., 2021b. Potassium phases and isotopic composition in modern marine biogenic carbonates. Geochim. Cosmochim. Acta 304, 364–380. https://doi.org/10.1016/j.gca.2021.04.018.

McCulloch, M.T., D'Olivo, J.P., Falter, J., Holcomb, M., Trotter, J.A., 2017. Coral calcification in a changing World and the interactive dynamics of pH and DIC upregulation. Nat. Commun. 8, 15686. https://doi.org/10.1038/ncomms15686.

Meibom, A., Cuif, J.P., Houlbreque, F., Mostefaoui, S., Dauphin, Y., Meibom, K.L., Dunbar, R., 2008. Compositional variations at ultra-structure length scales in coral skeleton. Geochim. Cosmochim. Acta 72 (6), 1555–1569. https://doi.org/10.1016/j.gca.2008.01.009.

Mergelsberg, S.T., De Yoreo, J.J., Miller, Q.R., Michel, F.M., Ulrich, R.N., Dove, P.M., 2020. Metastable solubility and local structure of amorphous calcium carbonate (ACC). Geochim. Cosmochim. Acta 289, 196–206. https://doi.org/10.1016/j.gca.2020.06.030.

Mitsuguchi, T., Kawakami, T., 2012. Potassium and other minor elements in Porites corals: implications for skeletal geochemistry and paleoenvironmental reconstruction. Coral Reefs 31 (3), 671–681. https://doi.org/10.1007/s00338-012-0902-3.

Montagna, P., McCulloch, M., Douville, E., López Correa, M., Trotter, J., Rodolfo-Metalpa, R., Dissard, D., Ferrier-Pagès, C., Frank, N., Freiwald, A., Goldstein, S., Mazzoli, C., Reynaud, S., Rüggeberg, A., Russo, S., Taviani, M., 2014. Li/Mg systematics in scleractinian corals: calibration of the thermometer. Geochim. Cosmochim. Acta 132, 288–310. https://doi.org/10.1016/j.gca.2014.02.005.

Montefalcone, M., Morri, C., Bianchi, C.N., 2018. Long-term change in bioconstruction potential of Maldivian coral reefs following extreme climate anomalies. Glob. Change Biol. 24, 5629–5641. https://doi.org/10.1111/gcb.14439.

Motai, S., Kawano, J., Nagai, T., Sowa, K., Watanabe, T., 2016. Precipitation of halite during calcification of the massive reef-building coral Porites lobata. Eur. J. Mineral. 28 (2), 265–271. https://doi.org/10.1127/ejm/2016/0028-2521.

Nielsen, L.C., DePaolo, D.J., De Yoreo, J.J., 2012. Self-consistent ion-by-ion growth model for kinetic isotopic fractionation during calcite precipitation. Geochim. Cosmochim. Acta 86, 166–181. https://doi.org/10.1016/j.gca.2012.02.009.

Ohki, S., Irie, T., Inoue, M., Shinmen, K., Kawahata, H., Nakamura, T., Kato, A., Nojiri, Y., Suzuki, A., Sakai, K., Woesik, R.V., 2013. Calcification responses of symbiotic and aposymbiotic corals to near-future levels of ocean acidification. Biogeosciences 10, 6807–6814. https://doi.org/10.5194/bg-10-6807-2013.

Okumura, M., Kitano, Y., 1986. Coprecipitation of alkali metal ions with calcium carbonate. Geochim. Cosmochim. Acta 50, 49–58. https://doi.org/10.1016/0016-7037(86)90047-5.

Pingitore, N.E., Villalobos, J., Cruz-Jimenez, G., Wellington, G.M., 2001. Incorporation of Potassium in Scleractinian Coral Aragonite: Preliminary X-Ray Absorption Spectroscopy. AGU Spring Meeting Abstracts. 2001, V41B-04.

Ramos, D.P.S., Morgan, L.E., Lloyd, N.S., Higgins, J.A., 2018. Reverse weathering in marine sediments and the geochemical cycle of potassium in seawater: insights from the K isotopic composition ($^{41}K/^{39}K$) of deep-sea pore-fluids. Geochim. Cosmochim. Acta 236, 99–120. https://doi.org/10.1016/j.epsl.2020.116290.

Ravel, B., Newville, M., 2005. ATHENA, ARTEMIS, HEPHAESTUS: data analysis for X-ray absorption spectroscopy using IFEFFIT. J. Synchrotron Radiat. 12 (4), 537–541. https://doi.org/10.1107/S0909049505012719.

Reggi, M., Fermani, S., Landi, V., Sparla, F., Caroselli, E., Gizzi, F., Dubinsky, Z., Levy, O., Cuif, J.P., Dauphin, Y., Goffredo, S., Falini, G., 2014. Biomineralization in Mediterranean corals: the role of the intraskeletal organic matrix. Cryst. Growth Des. 14 (9), 4310–4320.

Saenger, C., Wang, Z., 2014. Magnesium isotope fractionation in biogenic and abiogenic carbonates: implications for paleoenvironmental proxies. Quat. Sci. Rev. 90, 1–21. https://doi.org/10.1016/j.quascirev.2014.01.014.

Schauble, E.A., 2004. Applying stable isotope fractionation theory to new systems. Rev. Mineral. Geochem. 55 (1), 65–111. https://doi.org/10.2138/gsrmg.55.1.65.

Sinclair, D.J., Williams, B., Risk, M., 2006. A biological origin for climate signals in corals - trace element "vital effects" are ubiquitous in Scleractinian coral skeletons. Geophys. Res. Lett. 33. https://doi.org/10.1029/2006GL027183.

Stan, C.V., Marcus, M.A., Gilbert, P.U.P.A., 2017. Amorphous calcium carbonate particles form coral skeletons. Proc. Natl. Acad. Sci. USA 114, E7670–E7678. https://doi.org/10.1073/pnas.1707890114.

Stanley, G.D., 1988. The history of early Mesozoic reef communities; a three-step process. Palaios 3 (2), 170–183. https://doi.org/10.2307/3514528.

Stanley, S.M., 2008. Effects of global seawater chemistry on biomineralization: past, present, and future. Chem. Rev. 108 (11), 4483–4498. https://doi.org/10.1021/cr800233u.

Sun, C.Y., Stifler, C.A., Chopdekar, R.V., Schmidt, C.A., Parida, G., Schoeppler, V., Fordyce, B.I., Brau, J.H., Mass, T., Mass, S., Gilbert, P.U., 2020. From particle attachment to space-filling coral skeletons. Proc. Natl. Acad. Sci. USA 117, 30159–30170. https://doi.org/10.1073/pnas.2012025117.

Suwa, R., Nakamura, M., Morita, M., Shimada, K., Iguchi, A., Sakai, K., Suzuki, A., 2010. Effects of acidified seawater on early life stages of scleractinian corals (Genus Acropora). Fish. Sci. 7, 93–99. https://doi.org/10.1007/s12562-009-0189-7.

Suzuki, A., Hibino, K., Iwase, A., Kawahata, H., 2005. Intercolony variability of skeletal oxygen and carbon isotope signatures of cultured Porites corals: temperature-controlled experiments. Geochim. Cosmochim. Acta 69 (18), 4453–4462. https://doi.org/10.1016/j.gca.2005.05.018.

Ullmann, C.V., Korte, C., 2015. Diagenetic alteration in low-Mg calcite from macrofossils: a review. Geol. Q. 59, 3–20. https://doi.org/10.7306/gq.1217.

Von Euw, S., Zhang, Q., Manichev, V., Murali, N., Gross, J., Feldman, L.C., Gustafsson, T., Flach, C., Mendelsohn, R., Falkowski, P.G., 2017. Biological control of aragonite formation in stony corals. Science 356, 933–938. https://doi.org/10.1126/science.aam6371.

Wall, M., Fietzke, J., Crook, E.D., Paytan, A., 2019. Using B isotopes and B/Ca in corals from low saturation springs to constrain calcification mechanisms. Nat. Commun. 10 (1), 1–9. https://doi.org/10.1038/s41467-019-11519-9.

Wang, K., Close, H.G., Tuller-Ross, B., Chen, H., 2020. Global average potassium isotope composition of modern seawater. ACS Earth Space Chem. 4 (7), 1010–1017. https://doi.org/10.1021/acsearthspacechem.0c00047.

Wang, K., Peucker-Ehrenbrink, B., Chen, H., Lee, H., Hasenmueller, E.A., 2021. Dissolved potassium isotopic composition of major world rivers. Geochim. Cosmochim. Acta 294, 145–159. https://doi.org/10.1016/j.gca.2020.11.012.

Weiner, S., Dove, P.M., 2003. An overview of biomineralization processes and the problem of the vital effect. Rev. Mineral. Geochem. 54 (1), 1–29. https://doi.org/10.2113/0540001.

White, A.F., 1977. Sodium and potassium coprecipitation in aragonite. Geochim. Cosmochim. Acta 41 (5), 613–625. https://doi.org/10.1016/0016-7037(77)90301-5.

Yoshimura, T., Tanimizu, M., Inoue, M., Suzuki, A., Iwasaki, N., Kawahata, H., 2011. Mg isotope fractionation in biogenic carbonates of deep-sea coral, benthic foraminifera, and hermatypic coral. Anal. Bioanal. Chem. 401 (9), 2755–2769. https://doi.org/10.1007/s00216-011-5264-0.

Yoshimura, T., Tamenori, Y., Suzuki, A., Kawahata, H., Iwasaki, N., Hasegawa, H., Nguyen, L.T., Kuroyanagi, A., Yamazaki, T., Kuroda, J., Ohkouchi, N., 2017. Altervalent substitution of sodium for calcium in biogenic calcite and aragonite. Geochim. Cosmochim. Acta 202, 21–38. https://doi.org/10.1016/j.gca.2016.12.003.

Zhao, M., Tarhan, L.G., Zhang, Y., Hood, A., Asael, D., Reid, R.P., Planavsky, N.J., 2021. Evaluation of shallow-water carbonates as a seawater zinc isotope archive. Earth Planet. Sci. Lett. 553, 116599. https://doi.org/10.1016/j.epsl.2020.116599.